Magnetic properties of nickel nanowires: Effect of deposition temperature

Kafil M. Razeeb, Fernando M. F. Rhen, and Saibal Roy

Articles you may be interested in

Magnetic properties of nickel nanowires: Effect of deposition temperature

Kafil M. Razeeb, Fernando M. F. Rhen, and Saibal Roy[a)]
Tyndall National Institute, Lee Maltings, Prospect Row, Cork, Ireland

We have investigated the magnetic properties of electroplated nickel nanowires with very distinct nanostructures, which are obtained by simply changing the plating temperature of the electrolyte. Low temperature (40 °C) resulted in larger average grain size comparable to the diameter of the wires, whereas higher temperature (60 °C) revealed self-similar morphology composed of nanogranules. For low temperature samples, a two stage magnetization process is evident in the easy axis direction where grain size is comparable to wire diameter. In contrast, for high temperature samples, nanowires are formed by an agglomeration of particles with average diameter of about 22 nm. In this case each individual particle behaves as a single domain and thereby magnetization reversal occurs by the switching of an ensemble of randomly oriented particles and magnetization saturates quickly with applied field. In the present case, with the high density of disorder caused by the self-similar morphology of the nanogranules, we suggest that the switching mechanism of the magnetization occurs by localized coherent rotation, resulting in lower coercivity. This delineates first experimental evidence of three dimensional cooperative magnetic interactions among the nanogranules within self-similar morphology of nanowires in both parallel and perpendicular wire axes. © *2009 American Institute of Physics*. [DOI: 10.1063/1.3109080]

I. INTRODUCTION

Magnetic nanowires are a subject of topical interest due to their potential application as high density data storage and magnetic sensors and also due to their intricate magnetic properties. Among them, nickel nanowires were investigated by several groups mainly focusing on the correlation between the dimension of the wire and the hysteresis behavior,[1–3] effect of electrodeposition process parameters such as *p*H of the solution[3] on crystallographic orientation, and micromagnetic simulation to investigate the magnetic interaction of the nanowires embedded inside hexagonal arrangements.[4,5] However, the effect of deposition parameters such as temperature of the electrolyte on the structural morphology of nanowires and how they influence the magnetic properties were not studied in detail, though it was reported that different bath temperatures allowed different crystal orientations inside the nanowires and resulted in different grain sizes.[6] Skomski *et al.* studied the effect of grain size on the magnetic properties in polycrystalline nanowires and proposed a model for magnetic phase diagram of nanowires.[7] Most of these nanowires have an average diameter ranging from 5 to 50 nm.[8,9] This paper describes the effect of deposition temperature on the grain morphology of nickel nanowires and its influence on the magnetic properties of the nanowires embedded inside nanochannel alumina (NCA) templates which were not reported before.

II. EXPERIMENTAL

For deposition inside the pores of NCA templates, the one side of the template was first deposited with a conductive 500 nm aluminum using evaporation method. Ohmic contact to the substrate was made using Radionics silver conductive paint on, which has a volume resistivity of 0.001 Ω cm when fully hardened. The schematic of Fig. 1 shows the electroplating setup for the deposition of Ni nanowires inside alumina templates. A bath comprising of 53.643 g l^{-1} NiSO$_4\cdot$6H$_2$O and 30 g l^{-1} H$_3$BO$_3$ was prepared. De-ionized water with resistivity ~18 MΩ was used to prepare the solution. The *p*H of the solution was adjusted to 2.5 with addition of H$_2$SO$_4$ and stirred at a constant rpm of 660. The nickel nanowires were prepared inside the NCA template having three different nominal pore diameters of 200, 100, and 20 nm. The electrolyte temperature was maintained at 40 and 60$\pm$0.2 °C to prepare two batches of samples [henceforth regarded as "low temperature" (40 °C) and "high temperature" (60 °C) samples] using an ETS D-4
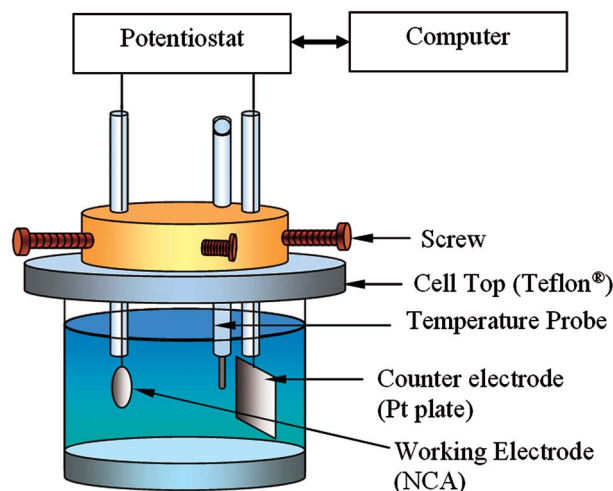

FIG. 1. (Color online) Schematic of electrodeposition setup for growing Ni nanowires inside alumina templates.

[a)]Author to whom correspondence should be addressed. Tel.: +353 21 4904331; FAX: +353 21 4270271. Electronic mail: saibal.roy@tyndall.ie.

Fuzzy IKA WERKE temperature controller. The bath was operated at a current density of 10 mA cm^{-2}. After deposition, the samples were thoroughly rinsed with de-ionized water and dried with nitrogen gun.

In terms of current efficiency, it is evident that the current efficiency is higher while depositing from high pH electrolyte at all cathode current densities.[10] An investigation was carried out to investigate the effect of pH on nickel deposits. Increasing the electrolyte pH from 2 to 3.5 while improving the current efficiency was detrimental to the deposit morphology. Cracking, curling, and the appearance of a second phase, an oxide or hydroxide, also accompanied with the increase in electrolyte pH. A low pH value of 2.0 did have a high quality deposit when both the temperature and nickel (Ni^{2+}) concentration were kept at 40 °C and 40 g l^{-1}, respectively, but the current efficiency decreased to 71%.[11] Therefore, the pH of the bath was set to 2.5 and it showed high quality of deposit.

The pore filling of nickel was investigated by Hitachi S4000 scanning electron microscope (SEM). Transmission electron microscope (TEM) was used to study the nanostructure of the nickel wires. Cross section of the samples was prepared by focused ion beam (FIB) milling for TEM observation. The grain size distribution was obtained by counting and measuring the grain diameters from micrograph using ImageJ software. For further estimation of overall grain size and crystal orientation X-ray diffraction (XRD) measurements were carried out using a Philips PW3710 diffractometer with Cu $K\alpha_1$ radiation, having a wavelength of 1.540 56 Å. The magnetic properties were investigated using a MPMS XL5 Superconducting quantum interference device (SQUID) with an applied field up to 5 T.

III. RESULTS AND DISCUSSION

Commercially available NCA samples named Anodisc™ 25 by Whatman plc© having three different nominal pore sizes (200, 100, and 20 nm) called NCA200, NCA100, and NCA20, respectively, are used in the present study. In order to measure the average pore size of NCAs, SEM images were analyzed with image analysis software named QUARTZ PCI-IMAGE MEASUREMENT SYSTEM. For NCA200, the average pore diameter on the "filtration side" is 209.4 nm whereas that on the "reverse side" is 308.5 nm. There is a deviation from circularity for most of the pores.[12] The average pore diameter for NCA100 is found to be 112 nm on the filtration side and 242 nm on the reverse side, whereas for NCA20 the average pore diameters on the filtration and the reverse side are 30 nd 202 nm, respectively. This heterogeneity in the pore structure of the NCA is created by varying the process parameters during the fabrication of the membranes. Different anodizing voltages were applied to the pure aluminum metal substrate during the growth of the NCA; thus in effect large pores extend virtually through the whole bulk of the oxide, except for a thin layer at one end where small pores prevail.[13] A long-range hexagonal arrangement of pores can be established for the pores, though pentagonal and heptagonal arrangements can also be observed. These arrangements are due to the mechanism of the pore growth during anodization of the aluminum substrate.[14] Hexagonal arrangements results from the hcp basal plane of the starting aluminum foil and the attrition due to anodization, which starts from the center and the six corners of the hexagonal base. Pentagonal arrangement results when two of the surrounding pores are fused together and heptagonal arrangement can result when a pore has suffered incomplete attrition compared to others. Barnard et al.[15] calculated the width of the walls from the porosity data provided by the manufacturer assuming an ideal hexagonal array of pores. The values obtained in this way are only for the filtration side of the NCA and are compared with our observations from SEM. The thicknesses of the pore walls obtained in this study are in good agreement with the theoretical values calculated by Barnard et al. which reported 69, 50, and 15–18 nm for NCA200, NCA100, and NCA20 templates. However, on the reverse side, the average thickness of the walls show different values of 112, 96, and 92 nm for NCA200, NCA100, and NCA20 templates, respectively. To define the matrix of nanowires in alumina, the width of the pore wall is important since it actually reveals what will be the separation among the nickel nanowires inside the alumina matrix. In order to understand the magnetic interaction among the nickel nanowires, the separation among the wires needs to be measured, which turns out to be the width of the pore walls. Since, the amount of pentagonal arrangement within hexagonally arranged nanowires is ~1%–2%,[12,16] it can be ignored as an effect on the overall magnetic behavior.

The effect of random disorder (from an ideally ordered hexagonal array) and surface morphology of nickel nanowires on magnetic properties was investigated by several groups.[17–19] It was shown by simulation that the random disorder resulted in the requirement of higher magnetic field to reach saturation when compared to ideal hexagonal array. Due to the disorder in some places, the nanowires come closer to each other and a dipole-dipole asymmetric interaction governs the requirement of larger magnetic field to reach saturation and resulted in a reduced remanence, while coercivity remained unchanged.[17]

While measuring magnetization process using SQUID magnetometer we measured the overall magnetic properties of any sample. Since the length of the branched filtration side of the template is only 3−5 μm as opposed to the overall 60 μm and as the aspect ratio (length/diameter) of the nanowires is quite high (~200), the influence of disorder of nanowires on magnetic behavior is not evident in the magnetic measurements. Furthermore, the effect of the random disorder in the hexagonal arrangement and the deviation in the circularity of the nickel nanowires on the overall magnetic properties are nullified in the present study due to the use of the same templates to fabricate these nanowires.

A. Electron microscopy

Figure 2(a) shows the SEM image of the nickel nanowires embedded inside alumina after the template was partially removed by NaOH etching. The image was taken at a 45° angle to the template. Figure 2(b) shows a typical SEM image of the top of nickel nanowires fabricated at 40 °C
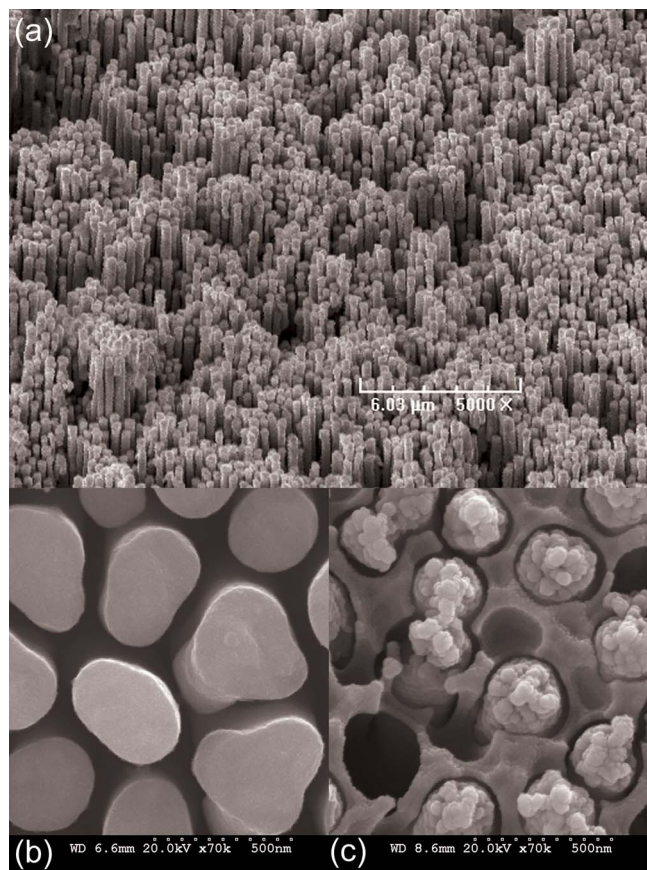
FIG. 2. (Color online) (a) High density Ni nanowires embedded inside partially etched alumina. (b) SEM of top of the nickel nanowires deposited at 40 °C in NCA200 template where the wires came out of the pores. (c) Nickel nanowires deposited at 60 °C.

posited templates confirmed that nearly 95% pores of the NCA were filled with nickel. Hence, the Ni volume fraction in each NCA sample was considered to be similar to the porosity value of that template, which is 50% for NCA200.

TEM analysis revealed a wide range of grain sizes in nickel nanowires. Figure 3(a) shows the dark field image of low temperature sample with corresponding selected area diffraction (SAD) pattern in the inset. Grain size ~150 nm was visible in several areas of individual wires. Some of the metal grains were found to be faceted as at E in Fig. 3(a) that extends across the diameter of the wire. The SAD pattern showed in the inset of Fig. 3(a) confirmed the polycrystalline nature of the nanowires with diffraction pattern matching the face centered cubic (fcc) Ni. The (111) and (200) spacings of fcc Ni was marked at Y and Z, respectively. Figure 3(b) shows the dark field TEM image of a single crystal Ni grain that has reasonably high density of fine dislocations. The reflections in the diffraction pattern are for (111) Ni spacings. From histogram analysis the mean diameter was measured around 108 nm as shown in Fig. 3(c). Figure 3(d) shows the bright field image of nickel nanowires fabricated at a deposition temperature of 60 °C. To delineate the inherent morphology of each individual nanowire, the cross sections were obtained by FIB milling from the middle of the wires, which is shown in Fig. 3(e). It is surprising to note that higher deposition temperature resulted in ultrafine grain structure with average size of 22 nm, where the size of maximum number of grains is ~10 nm as analyzed in the histogram of Fig. 3(f). This necessarily means that self-similar growths observed in SEM images were mainly composed of nanogranules, formed by the random walk of depositing ion as evidenced in the case of other diffusion limited aggregation processes.[20,21]

B. Magnetic properties

The nickel nanowires grown inside the alumina templates can be qualitatively classified according to the predicted magnetic phase diagram[7] which shows crossover from

inside NCA200 template. The nickel wires in NCA200 typically have diameters that are comparable to the pore diameter. The density of the wires is about 10^8 cm^{-2}. Figure 2(c) shows the sample fabricated from 60 °C electrolyte where self-similar growth can be observed in each individual nanowire. SEM observation on different areas of the electrode-
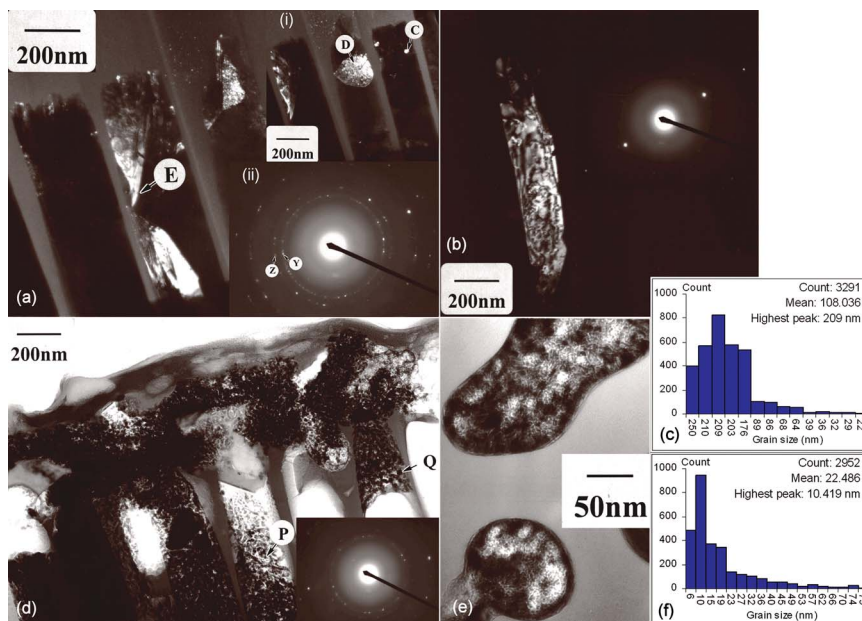

FIG. 3. (Color online) (a) Dark field TEM image showing large faceted grains for nanowires deposited at 40 °C. Insets: (i) shows spherical grains at D; (ii) SAD pattern reveals the polycrystalline nature of nickel, showing (111) and (200) spacings. (b) Single crystal grain showing high density of fine dislocations and the corresponding SAD pattern. (c) Grain size histogram analysis of 40 °C sample. (d) Bright field TEM image of Ni nanowires deposited at 60 °C showing fine grain structures and the corresponding SAD pattern (inset). (e) A plan view section from midthickness region of 60 °C sample showing fine grains confirmed that the grain size is homogeneous throughout the wires. (f) Grain size histogram analysis of 60 °C sample.
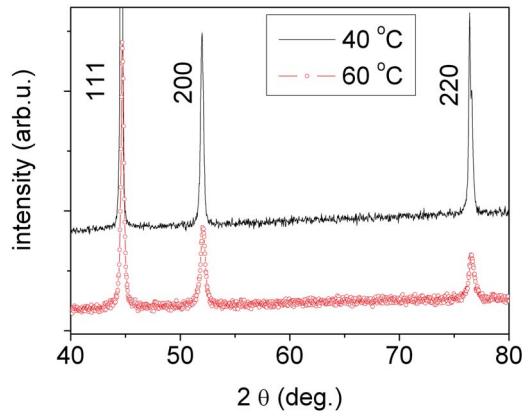
FIG. 4. (Color online) Diffraction pattern of Ni nanowire electroplated at 40 and 60 °C. Peaks correspond to fcc Ni.

cooperative to noncooperative magnetic interactions with respect to their crystallite sizes and wire diameters. According to the phase diagram, in the present work, wires deposited at 40 °C should exhibit three dimensional noncooperative interactions because of their grain size (~108 nm) which is comparable to the wire diameter and much higher than the domain wall width, whereas samples plated at 60 °C are supposed to show three dimensional cooperative interactions, which has average grain size of 22 nm, lower than the domain wall width.

TEM and XRD results indicate that nickel nanowires are polycrystalline as shown in Figs. 3 and 4. Therefore, the magnetocrystalline anisotropy contribution to the hysteretic behavior needed to be evaluated. The following equation was used to determine the effect of magnetocrystalline anisotropy contribution in comparison to shape anisotropy contribution:[22,23]

$$K_{eff} = pK_1 + \pi p M_s^2 (1 - 3p), \qquad (1)$$

where p is the geometric packing density for ideal hexagonally arranged array of pores, K_{eff} is the effective anisotropy constant, K_1 is the magnetocrystalline anisotropy constant (for nickel it is -4.5×10^3 J m^{-3}), and M_s is the saturation magnetization of nickel. For a hexagonal array of nanowires:[23]

$$p = \frac{\pi}{(2\sqrt{3})(D_p/D_{cell})^2}. \qquad (2)$$

Here D_p is the pore diameter and D_{cell} is the hexagonal cell diameter. An illustration of the effect of the crystalline anisotropy in the effective anisotropy (K_{eff}) is shown in Fig. 5 as a function of packing density of nickel nanowire in alumina matrix. The solid line is solely determined by the shape anisotropy and the influence of the crystal anisotropy shifts the line to lower or higher values assuming solely parallel or perpendicular crystal anisotropy with K_1 value for bulk nickel, that is, (111) plane parallel or perpendicular to the nanowire axis. So it can be concluded that the crystal anisotropy has little or no effect compared with that of the shape anisotropy. This is due to the fact that in case of nickel nanowires, the shape anisotropy constant ($K_s = 7.4 \times 10^4$ J m^{-3}) is one order of magnitude greater than the crystalline anisotropy constant ($K_1 = -4.5 \times 10^3$ J m^{-3}) and opposite in sign. As a result the effective anisotropy field is only due to the shape anisotropy in the nickel nanowire matrix and can be written as $H_{keff} = H_{ks} = 2\pi M_s = 242.057$ kA m^{-1} (3041.7 Oe).

The comparison between crystalline and magnetoelastic anisotropies is frequently used for continuous films and bulk sample of Ni. In case of nanowire grown in porous template, the contribution to magnetoelastic anisotropy arises mainly from the mismatch of thermal expansion coefficients of metallic nanowires and the ceramic/polymer matrix. These are apparent in reported samples measured from room temperature to ~5 K.[19,24,25] In the present study all the magnetic measurements were carried out at room temperature (~300 K) generating negligible magnetoelastic anisotropy compared to lower temperature. However, the strain of the samples fabricated at two different temperatures (40 and 60 °C) was calculated from the slow scan XRD. Lattice expansion or contraction is usually expressed in terms of $\Delta a/a_0$, where a_0 is the lattice constant of the strain-free material. $\Delta a/a_0$ is related to macrostrain (mean strain) ε and deformation stacking fault probability α' as $\Delta a/a_0 = \varepsilon + G\alpha'$, where G is a constant depending on (hkl) and the structure of the material.[26] However, the occurrence of the deformation faults in thin films is negligible.[27] So, the sec-
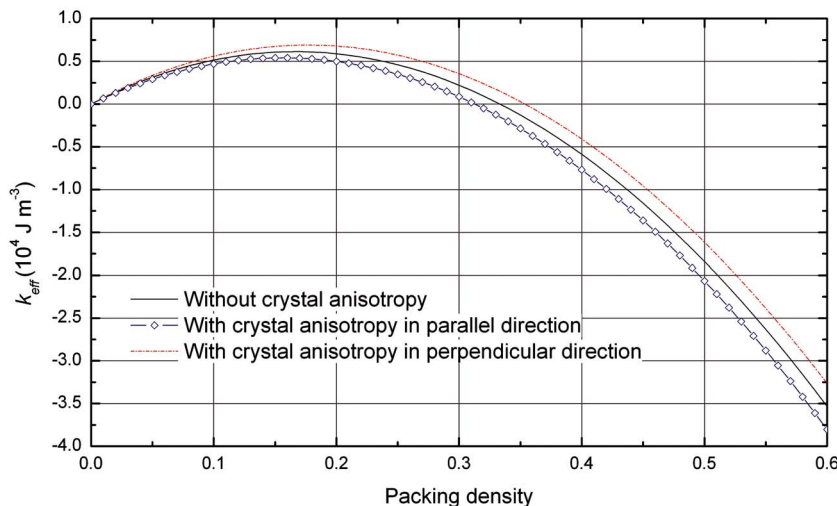

FIG. 5. (Color online) Effective magnetic anisotropy for nickel nanowire array as a function of packing density showing small variation with and without crystal anisotropy.
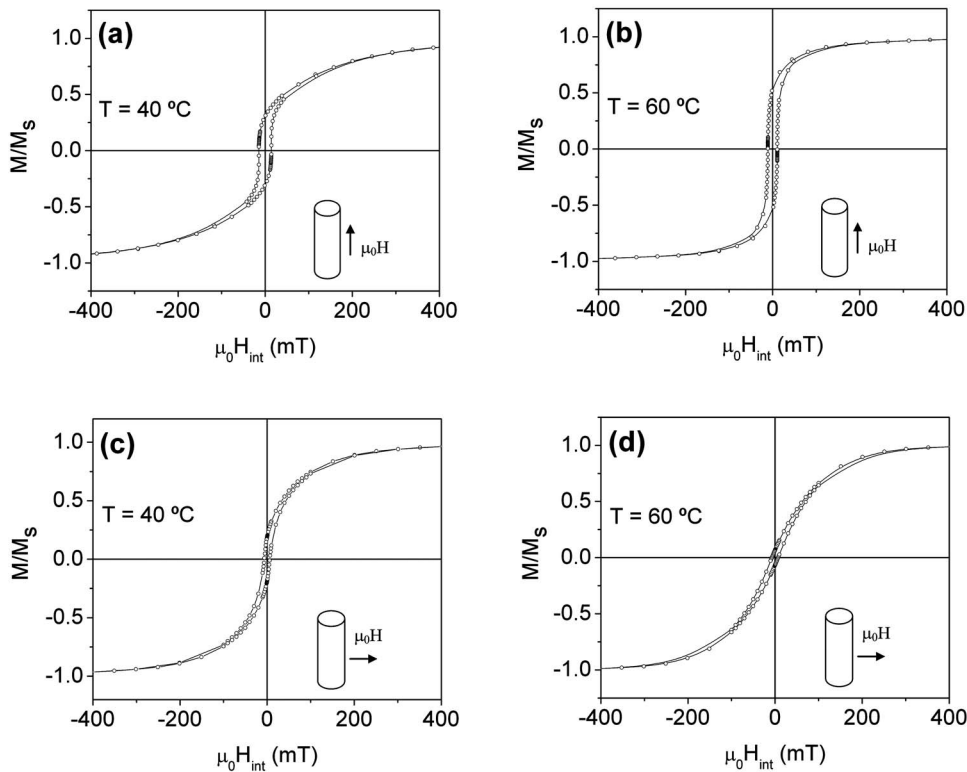
FIG. 6. Room temperature magnetization curves measured along Ni nanowire electroplated into 200 nm alumina pores templates when field is applied parallel and perpendicular to the wire axes fabricated at [(a) and (c)] 40 °C and [(b) and (d)] 60 °C electrolyte temperatures.

ond term in the above equation can be ignored. The strain component ε_n normal to the film surface can therefore be calculated directly from the lattice constants a and a_0. The macrostrain values obtained for low and high temperature samples are about ~0.1% and hence we neglected the magnetoelastic contribution to anisotropy in both cases.

Room temperature magnetization curves of electroplated Ni nanowires prepared at different temperatures are shown in Fig. 6. The internal field (H_{int}) is obtained using demagnetizing field correction according to the equation $H_{int}=H_{ext}-D_{eff}M$. Here, we use an effective demagnetizing field[28] $D_{eff}=D+f(D'-D)$, where D is the demagnetizing factor of an individual wire, D' is the overall demagnetizing factor for the membrane, and f is the fill factor (0.7). Thereby, we obtain effective demagnetizing factors $D_{eff}^{\perp}=0.7$ and $D_{eff}^{\parallel}=0.15$, along and perpendicular to the wire axis, respectively.

The comparison between low and high temperature samples revealed that when deposition occurred from an electrolyte having solution temperature of 60 °C, the orientation showed the peak intensities as $(111)>(200)>(220)$. Deposition from a lower bath temperature (40 °C) showed an orientation as $(111)>(220)>(200)$. The wires deposited at 40 °C showed a stronger (220) preferred orientation as opposed to (200) at 60 °C. The magnetic easy and hard axes of bulk Ni lie along the [111] and [100] directions, respectively.[29] XRD patterns of both samples prepared at 40 and 60 °C (Fig. 4) show a preferential texture [111] compared to [200] and [220]. The [111] direction being the same as the wire growth, it is expected that the easy axis will lie along the nanowire. On the other hand, for 60 °C sample, the (200) peak being more intense as oppose to (220), the growth along the hard direction [100] was more preferred than the 40 °C sample. This justifies the nanogranular

growth leading to self-similar morphology in 60 °C samples, whereas large single crystalline growth along the wire direction was observed in 40 °C samples. This is further corroborated from the magnetic measurements as depicted in the later section.

Magnetization of the wire shows systematically a slow dependence on field for $H_{int}>H_c$ [Fig. 6(a)] in samples prepared at low temperature (40 °C), which can be interpreted in terms of microstructure of the deposits. Sample prepared at low temperature consists of long continuous polycrystalline wires with length of up to 60 μm. The typical domain wall width, $l_w=2\,(A/K_1)^{1/2}$ (where A is the exchange stiffness) of Ni is about 22–28 nm,[30] and thereby the multidomain structure within a single wire is likely to form. In fact, single domain nanowires are usually obtained in wire with diameter smaller or the same order as l_w (26 nm) and show coercivity of about 100 mT.[31,32] We obtained coercivity values of 7–15 mT for low temperature samples (having grain size of the order of 108 nm), which are about ten times smaller than single domain coercivity. The magnetization reversal mechanism occurred by nucleation followed by domain propagation along the easy axis. There is a considerable density of defects in large crystallites (Fig. 3), so it requires a larger magnetic field to fully align the magnetization. The propagation of the domain is pinned by the crystallographic defects and the magnetization slowly saturates with applied field.

In contrast, high temperature samples showed a coercivity of 5–10 mT (see Fig. 7). In case of constricted growth of nanowires within porous membrane, it was reported that when the diameter of the nanowires is greater 50 nm, curling is the preferred magnetization reversal mechanism and when the diameter of the nanowire is less than 30 nm, the magne-
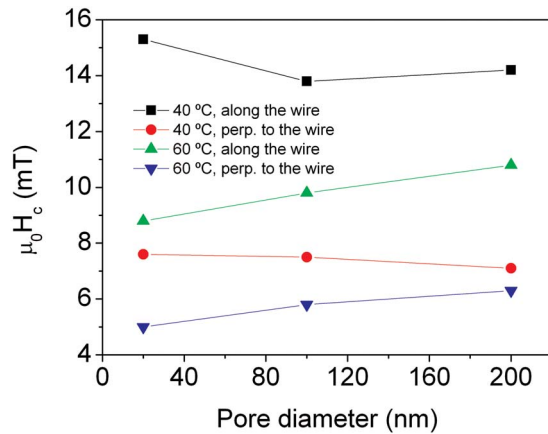
FIG. 7. (Color online) Coercivity dependence on pore diameter (nominal) and plating temperature.

tization reversal mechanism switches to coherent rotation.[33] In high temperature samples the wires are formed by an agglomeration of particles with an average diameter of 22 nm (the maximum number of grains is ~10 nm), which is lower than domain wall size. In this case, the magnetic behavior can be understood in terms of an ensemble of fine particles with relatively random easy axis orientation. Therefore, the switching mechanism is supposed to occur by continuous rotation of magnetization as in a single domain particle. However, due to the imperfections caused by the nanostructures, the reversal mode seems to be localized, which reduces the coercivity.[34] The localization length depends on the wire nanostructure, which goes to infinity for zero disorder and reversal mechanism leads to coherent rotation. In the present case, with the high density of disorder caused by the self-similar morphology of the nanogranules, we suggest that the switching mechanism of the magnetization occurs by localized coherent rotation, resulting in lower coercivity. This can be further corroborated by comparing the four hysteresis loop shown in the Fig. 6 where the low temperature sample showed two distinct hysteresis behaviors for field applied parallel and perpendicular to the wire axis. A single stage magnetization curve was obtained for perpendicular applied field compared to the two stage magnetization behavior in case of parallel applied field. On the other hand, in the 60 °C (high temperature) sample, for parallel and perpendicular applied fields, the hysteresis curves showed surprising similarity where both the curves have single slope magnetization. This is due to the self-similar growth of nickel inside the wires, which again are composed of nanogranules having average particle diameter of 22 nm comparable to the domain wall width. These high temperature nickel wires composed of nanometric crystallites are believed to reduce the effect of shape anisotropy as observed in high aspect ratio nanowires and resulted in comparable magnetization curves for field applied parallel and perpendicular to the wire axis. This delineates the first experimental evidence of three dimensional cooperative magnetic interactions among the nanogranules within self-similar morphology of nanowires in both parallel and perpendicular directions.

IV. CONCLUSIONS

In conclusion, we have fabricated nickel nanowires at two different deposition temperatures which influenced the grain structure of the nickel inside the nanowires. The crystal orientation was a function of deposition temperature as well as pore diameter. Magnetic hysteretic behavior showed grain size dependence. The propagation of the domain is pinned by the defects and a two stage magnetization curve was observed for low temperature samples where the grain size is comparable to the wire diameter. In case of high temperature samples, the grain size is comparable to the domain wall size of nickel, where an individual grain behaves as a single domain and thereby the switching mechanism occurs by continuous rotation of magnetization resulting in a single slope.

ACKNOWLEDGMENTS

[1] T. M. Whitney, J. S. Jiang, P. C. Searson, and C. L. Chien, Science **261**, 1316 (1993).
[2] K. Nielsch, R. B. Wehrspohn, J. Barthel, J. Kirschner, U. Gosele, S. F. Fischer, and H. Kronmuller, Appl. Phys. Lett. **79**, 1360 (2001).
[3] I. Z. Rahman, K. M. Razeeb, M. A. Rahman, and Md. Kamruzzaman, J. Magn. Magn. Mater. **262**, 166 (2003).
[4] I. Z. Rahman, A. Boboc, K. M. Razeeb, and M. A. Rahman, J. Magn. Magn. Mater. **290–291**, 246 (2005).
[5] R. Hertel, J. Magn. Magn. Mater. **249**, 251 (2002).
[6] K. M. Razeeb and S. Roy, J. Appl. Phys. **103**, 084302 (2008).
[7] R. Skomski, H. Zheng, M. Zheng, and D. J. Sellmyer, Phys. Rev. B **62**, 3900 (2000).
[8] P. M. Paulus, F. Luis, M. Kröll, G. Schmid, and L. J. de Jongh, J. Magn. Magn. Mater. **224**, 180 (2001).
[9] D. J. Sellmyer, M. Zheng, and R. Skomski, J. Phys.: Condens. Matter **13**, R433 (2001).
[10] I. Epelboin, M. Jousellin, and R. Wiart, J. Electroanal. Chem. Interfacial Electrochem. **119**, 61 (1981).
[11] M. Holam and T. J. O'Keefe, Minerals Eng. **13**(2), 193 (2000).
[12] K. M. Razeeb, I. Z. Rahman, and M. A. Rahman, J. Metastable Nanocryst. Mater. **17**, 1 (2003).
[13] I. Z. Rahman, K. M. Razeeb, Md. Kamruzzaman, and M. Serantoni, J. Mater. Process. Technol. **153–154**, 811 (2004).
[14] J. P. O'Sullivan and G. C. Wood, Proc. R. Soc. London, Ser. A **317**, 511 (1970).
[15] J. A. Barnard, N. Fujiwara, V. R. Inturi, J. D. Jarratt, T. W. Scharf, and J. L. Weston, Appl. Phys. Lett. **69**, 2758 (1996).
[16] K. M. Razeeb, Ph.D. thesis, University of Limerick, 2003.
[17] M. Vázquez, M. Hernández-Vélez, K. Pirota, A. Asenjo, D. Navas, J. Velázquez, P. Vargas, and C. Ramos, Eur. Phys. J. B **40**, 489 (2004).
[18] M. Vázquez, K. Nielsch, P. Vargas, J. Velázquez, D. Navas, K. Pirota, M. Hernández-Vélez, E. Vogel, J. Cartes, R. B. Wehrspohn, and U. Gösele, Physica B **343**, 395 (2004).
[19] H. Zeng, S. Michalski, R. D. Kirby, D. J. Sellmyer, L. Menon, and S. Bandyopadhyay, J. Phys.: Condens. Matter **14**, 715 (2002).
[20] S. Roy and D. Chakravorty, Appl. Phys. Lett. **59**, 1415 (1991).
[21] S. Roy and D. Chakravorty, Phys. Rev. B **47**, 3089 (1993).
[22] H. Schwanbeck and U. Schmidt, Electrochim. Acta **45**, 4389 (2000).
[23] L. Cheng-Zhang and J. C. Lodder, J. Magn. Magn. Mater. **88**, 236 (1990).
[24] D. Navas, K. R. Pirota, P. Mendoza Zelis, D. Velazquez, C. A. Ross, and M. Vazquez, J. Appl. Phys. **103**, 07D523 (2008).
[25] J. D. L. T. Medina, M. Darques, and L. Piraux, J. Phys. D **41**, 032008 (2008).

[26]C. N. J. Wagner, A. S. Tetelman, and H. M. Otte, J. Appl. Phys. **33**, 3080 (1960).

[27]M. Hecq, A. Hecq, and J. L. Langford, J. Appl. Phys. **53**, 421 (1982).

[28]R. Skomski and J. M. D. Coey, *Permanent Magnet* (IOP, Bristol, 1999).

[29]J. Trygg, B. Johansson, O. Eriksson, and J. M. Wills, Phys. Rev. Lett. **75**, 2871 (1995).

[30]M. E. Schabes, J. Magn. Magn. Mater. **95**, 249 (1991).

[31]K. Nielsch, R. B. Wehrspohn, J. Barthel, J. Kirschner, S. F. Fischer, H. Kronmuller, T. Schweinbock, D. Weiss, and U. Gosele, J. Magn. Magn. Mater. **249**, 234 (2002).

[32]A. Asenjo, M. Kaafar, D. Navas, and J. Vazquez, Appl. Phys. (Berl.) **100**, 023909 (2006).

[33]G. C. Han, B. Y. Zong, P. Luo, and Y. H. Wu, J. Appl. Phys. **93**, 9202 (2003).

[34]R. Skomski, H. Zeng, and D. J. Sellmyer, J. Magn. Magn. Mater. **249**, 175 (2002).